JTTEE5 11:409–414

Use of Plasma Spraying in the Manufacture of Continuously Graded and Layered/Graded Molybdenum Disilicide/Alumina Composites

Rajendra U. Vaidya, Richard G. Castro, Maria I. Peters, David E. Gallegos, and John J. Petrovic

(Submitted 10 December 2000; in revised form 24 January 2001)

Plasma spraying was used to produce continuously graded and graded/layered structures of molybdenum disilicide ($MoSi_2$) and alumina (Al_2O_3). These functionally graded materials (FGMs) were achieved by manipulating the powder hoppers and plasma torch translation via in-house created computer software. The resultant microstructures sprayed uniformly and were crack free. The interface between $MoSi_2$ and Al_2O_3 was continuous and no evidence of debonding or cracking at the interface was found. The mechanical strength of these sprayed materials was evaluated using C-ring samples (in diametrical compression). Weibull analysis conducted on the C-ring data indicated that the continuously graded samples were slightly stronger and had a significantly narrower strength distribution than the graded/layered samples. Although the average strength values of both types of functionally graded samples were closer to those of monolithic $MoSi_2$, the fracture energy of the graded samples was significantly larger (~2-3 times) compared with the monolithic materials. Scanning electron microscopy (SEM) conducted on the fracture surfaces of the FGMs illustrated a wavy and tortuous crack path through the composite cross section of the sample, with extensive crack kinking. This study has two important results. First, we demonstrated the ability to produce such functionally graded composite ceramic microstructures using a conventional plasma spraying process. Second, we quantified the improvements in mechanical performance provided by these FGMs over conventional monolithic materials.

Keywords C-ring test, functionally graded materials, $MoSi_2$, plasma spraying, Weibull modulus

1. Introduction

Requirements for high temperature applications in the glass industry such as temperature sensor sheaths and video sensor systems have fueled interest in molybdenum disilicide based materials. Molybdenum disilicide is a candidate high temperature material for such applications because of its high melting temperature (2030 °C), relatively low density (6.24 g/cm^3), high thermal conductivity (52 W/mK), a brittle to ductile transition near 1000 °C, and stability in a variety of corrosive and oxidative environments.[1-6] Molybdenum disilicide also exhibits excellent resistance to corrosion when immersed in molten glass. The major drawbacks of molybdenum disilicide limiting its widespread use in the glass industry are its inherent brittleness and modest strength at low temperatures (<1000 °C), its tendency to pest at intermediate temperatures (~500 °C), and its tendency to corrode at the glass line in immersion applications.[7]

To overcome some of these problems, plasma sprayed, continuously graded and graded/layered microstructures of molybdenum disilicide ($MoSi_2$) and alumina (Al_2O_3) were investigated. The continuously graded and graded/layered microstructures embrace the concept of functionally graded materials (FGMs), where a gradual change in composition is created to avoid sharp interfaces among brittle materials. Graded materials provide added advantages of smaller residual stresses, enhanced interfacial bonding, and reduced severity of stress concentrations at sharp interfaces.[8,9] Plasma spraying was used because it is a very versatile and efficient method for producing such complex FGM microstructures. Furthermore, large net shape components can be built up very rapidly using this process. Alumina was chosen as the coupling material for molybdenum disilicide because it has a coefficient of thermal expansion (CTE) and elastic modulus similar to that of molybdenum disilicide (CTE $MoSi_2 = 8 \times 10^{-6}$/°C, CTE $Al_2O_3 = 9.2 \times 10^{-6}$/°C; E_{MoSi2} = 320 GPa, E_{Al2O3} = 350 GPa). Studies on other brittle material systems have indicated that layered microstructures (where the mismatch in elastic and thermal properties is carefully controlled) can lead to significant improvements in strength and other mechanical properties.[8,9] Of particular significance are the results of a recent study[10] in which a large increase in damage tolerance was achieved by layering alumina with mullite. The damage tolerance (and flaw size insensitivity) achieved in these layered materials was attributed to compressive stresses in alternating layers of the laminar composite material.

The focus of this study was two-fold. First, we wished to demonstrate the capability of producing such graded and layered microstructures by manipulating the spray process variables. This was achieved by changing variables such as powder hopper speed, gas flow rate, and plasma torch head position and speed. Second, we were interested in comparing the mechanical perfor-

Rajendra U. Vaidya, Richard G. Castro, Maria I. Peters, David E. Gallegos, and **John J. Petrovic,** Materials Science and Technology Division, Los Alamos National Laboratory, Mail Stop E506, Los Alamos, NM 87545. Contact e-mail: raj@lanl.gov.

Table 1 Plasma Spraying Parameters Used in Fabricating the Composite Tubes

Plasma gun voltage:	25 V
Plasma gun current:	850 A
Gun to work distance:	7.5 cm
Arc and powder gas:	argon
Arc gas flow rate:	40 slpm
Powder gas flow rate:	variable (see Table 2 and the test for details)
Atmosphere:	air

mance of the continuously graded and graded/layered materials from an application perspective. To achieve that end, mechanical testing was performed using C-ring samples.

2. Experimental

Studies were conducted on cylindrically graded and graded/layered $MoSi_2$-Al_2O_3 samples. Two basic types of composite tubes were fabricated. The first type of tube had a continuously graded microstructure for which the composition was pure Al_2O_3 on the inside of the tube and pure $MoSi_2$ on the outside of the tube. The second sample consisted of a layered/graded microstructure. This sample also had a layer of pure Al_2O_3 on the inside of the tube and a layer of pure $MoSi_2$ on the outside of the tube. Sandwiched between the inner and outer layers were seven other discrete layers consisting of a fixed composition of $MoSi_2$ and Al_2O_3. There were a total of nine layers in this sample. In addition to these graded microstructures, we also sprayed monolithic samples of $MoSi_2$ and Al_2O_3. Dimensions and a few other details of the sprayed tubes are given below.

For sample type 1 (continuously graded microstructure), an area 31.75 mm in diameter was sprayed on a hollow 12.7 mm diameter graphite tube. The graphite tube was removed during sample machining.

For sample type 2 (layered/graded microstructure), an area 31.75 mm in diameter was sprayed on a hollow 12.7 mm diameter graphite tube. Each layer was ~1.1 mm thick. The innermost layer had a composition of ~100% Al_2O_3. The composition of each successive layer decreased in weight percent in Al_2O_3 and increased in weight percent in $MoSi_2$. The composition of the outermost layer was ~100% $MoSi_2$.

A thermal spraying system (SG 100 gun and two model 1264 programmable hoppers, Praxair/TAFA Surface Technologies, Seattle, WA) coupled to a 6-axis robotic system (model S-10, Fanuc, Rochester Hills, MI), in-flight particle analyzer (model DPV 2000, Technar, Kent, United Kingdom), and infrared (IR) camera (model TH 5104, Mikron, Richmond, KY) were used to spray the samples. Pure Al_2O_3 (105, Metco, Auburn, WA) and $MoSi_2$ (Cerac, Milwaukee, WI) powders were used in the process. The $MoSi_2$ powder was spherical and had an average particle size of 65 μm. The powder purity was 99.5%. X-ray diffraction (XRD) analysis indicated the presence of the tetragonal phase and a trace of Mo_5Si_3. The Al_2O_3 powder particles were angular, and their size ranged from 5-20 μm. The powder was 99.9% pure with traces of Fe_2O_3 impurities. The plasma spraying parameters are given in Table 1.

The powder hopper speeds and gas flows were manipulated to vary the proportions of Al_2O_3 and $MoSi_2$. These variables were determined through trial experiments conducted prior to spraying the samples. The relative compositions of the layers

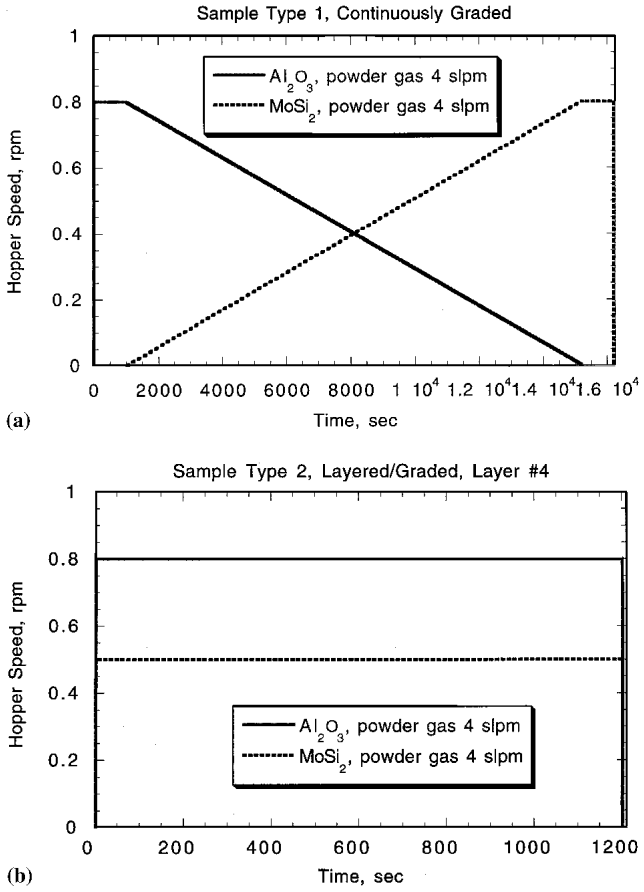

Fig. 1 Schematic of the program for the powder hoppers used in spraying **(a)** continuously graded microstructure and **(b)** layered and graded microstructure

were verified through energy dispersive spectroscopy (EDS). An outline of the hopper variables (gas flow rate and speed) is given below.

For sample type 1 (continuously graded microstructure), the powder hopper speed was ramped (up or down) from 0-0.8 rpm for both hoppers. The powder gas flow rate was 4 standard liters per minute (slpm) for both hoppers.

For sample type 2 (graded/layered microstructure), the powder hopper speed was 0.3, 0.5, or 0.8 rpm (depending on layer composition). The powder gas flow rate was 1, 2, or 4 slpm (depending on layer composition).

Figure 1(a,b) illustrates examples of the program for the powder hoppers used to spray the two samples. The list of the hopper speeds and gas flow rates for the various layers in sample type 2 are listed in Table 2. The powder hoppers used in the fabrication of these composite tubes were volume-feed type hoppers and increasing the rotational speed and powder gas flow rate increased the amount of powder fed into the plasma torch. The relationship between hopper speed and powder dispensing rate for the $MoSi_2$ and Al_2O_3 powders, at two different powder gas flow rates, can be seen in Fig. 2. The dispensing rate of the Al_2O_3 was significantly slower than that for the $MoSi_2$ (even after correcting for density), and was sensitive to the powder gas flow rate. Significant powder dispensing rates were only ob-

Table 2 Hopper Speed and Powder Gas Flow Rates Used in Spraying Sample Type 2

Layer No.	Al_2O_3 Hopper Speed, rpm	Al_2O_3 Gas Flow Rate, slpm	$MoSi_2$ Hopper Speed, rpm	$MoSi_2$ Gas Flow Rate, slpm	Time, s	Composition of Layer
1 (inner)	0.8	4.0	0	0	1600	100% Al_2O_3
2	0.8	4.0	0.3	2.0	1565	90% Al_2O_3, 10% $MoSi_2$
3	0.8	4.0	0.5	2.0	1450	82% Al_2O_3, 18% $MoSi_2$
4	0.8	4.0	0.5	4.0	1200	66% Al_2O_3, 34% $MoSi_2$
5	0.8	4.0	0.8	4.0	925	49% Al_2O_3, 51% $MoSi_2$
6	0.5	4.0	0.8	4.0	1065	31% Al_2O_3, 69% $MoSi_2$
7	0.5	2.0	0.8	4.0	1325	13% Al_2O_3, 87% $MoSi_2$
8	0.3	2.0	0.8	4.0	1465	6% Al_2O_3, 94% $MoSi_2$
9 (outer)	0	0	0.8	4.0	1510	100% $MoSi_2$

tained when the powder gas flow rate was ~4 slpm. On the other hand, the dispensing rate of the $MoSi_2$ powder exhibited a linear increase with hopper speed and was insensitive to the flow rate of the gas between 2 and 4 slpm.

2.1 Mechanical Testing

C-ring samples were wire electron discharge machined (EDM) out of the sprayed tube samples. The C-rings had an outer diameter (OD) of 25.93 mm, an inner diameter (ID) of 12.8 mm, and a width of 10.76 mm. The critical $b/(r_o - r_i)$ ratio (where b is the width of the sample, r_o is the outside radius and is equal to OD/2, and r_i is the inside radius and is equal to ID/2) was 1.64, within the required range of (1,4). The gap in the samples was equal to the width b of the samples. The C-ring samples were tested in diametrical compression using an hydraulic test frame (type 1331 with a 8500 plus controller and a 10 kN load cell, Instron, Canton, MA), at a cross-head speed of 0.125 mm/min (strain rate ~0.316×10^{-4} s^{-1}). Machine compliance was corrected using a standard Al_2O_3 sample of known stiffness. All of the samples were machined and tested in accordance with ASTM Standard C 1323-96. A total of 12 samples for each composite tube were tested. A total of three samples each of monolithic plasma sprayed $MoSi_2$ and Al_2O_3 were tested and used for comparison purposes only.

3. Results and Discussion

Optical micrographs of the cross sections of the sprayed tubes are shown in Fig. 3(a,b). The bonding between the various layers appeared to be excellent, with no evidence of cracking or delamination.

The maximum tensile stress at fracture was calculated from the load-displacement curves using the following equation (see ASTM Standard C 1323-96):

$$\sigma_{\theta max} = (PR/btr_o)\,[(r_o - r_a)/(r_a - R)] \quad \text{(Eq 1)}$$

where $\sigma_{\theta max}$ is the engineering tangential maximum hoop stress, P is the maximum applied compressive load, b is the specimen width, r_o is the outer radius of the ring, r_i is the inner radius of the ring, t is the specimen thickness (and is equal to $r_o - r_i$), r_a is the average radius and is equal to $(r_o + r_i)/2$, and R is defined as $(r_o - r_i)/\ln(r_o/r_i)$.

A Weibull statistical approach[11] was used to obtain the strength distributions of the samples. Although the standardized student t-test[12] employing the normal or gaussian frequency distribution is often used in statistical analysis, there is no theoretical or experimental justification for using it in problems involving fracture. Use of a normal distribution is often inappropriate in analyzing fracture problems with plasma sprayed ceramic materials because of the presence of multiple flaw populations. The Weibull distribution is more appropriate (and conservative) in this scenario because it does not require that the flaw population be normally distributed.

The Weibull approach is based on the weakest link theory,[11] and assumes that failure in the sample occurs from the largest flaw. The Weibull approach gives the probability of failure P at stress σ_f as

$$P(\sigma_f) = 1 - \exp\{-V_E[(\sigma_f - \sigma_u)/\sigma_o]^\beta\} \quad \text{(Eq 2)}$$

Here, V_E is the effective sample volume under stress, and is a function of the sample size and testing configuration, σ_o is a scale parameter, σ_u is the stress below which the probability of failure is zero, and β is the Weibull modulus. The Weibull modulus is an important parameter in characterizing the strength of brittle materials, and is a measure of the scatter in the strength of the material. In addition, the Weibull modulus is required to extrapolate data to predict the probability of failure of larger or smaller volumes of material under an applied stress.

Taking a conservative estimate of σ_u equal to zero, Eq 2 can be simplified to a two-parameter distribution as

$$P(\sigma_f) = 1 - \exp[-\alpha\sigma_f^\beta] \quad \text{(Eq 3)}$$

where α is a modified scaling parameter (equal to V_E/σ_o^β).

Taking the natural logarithm of Eq 3 twice and rearranging, we get

$$\ln\ln[1/(1 - P)] = \ln \alpha + \beta \ln \sigma_f \quad \text{(Eq 4)}$$

By plotting $\ln\ln[1/(1 - P)]$ against $\ln \sigma_f$, one can obtain the Weibull modulus β from the slope. The probability of failure P is obtained by arranging the strength values of the samples in ascending order, and assigning a probability of failure to each strength value using an estimator given by

$$P(\sigma_{fi}) = i/(1 + N) \quad \text{(Eq 5)}$$

where $P(\sigma_{fi})$ gives the probability of failure corresponding to the ith strength value, and N is the total number of samples tested.

The Weibull mean strength σ_f, standard deviation (SD) and coefficient of variation (CV) are given by

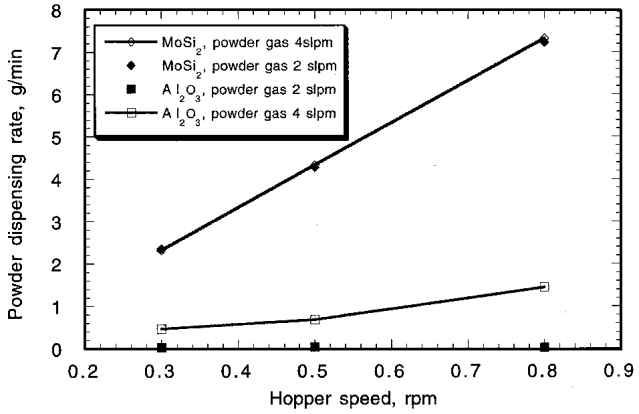

Fig. 2 Relationship between hopper speed and powder dispensing rate for the $MoSi_2$ and Al_2O_3 powders, as a function of powder gas flow rate

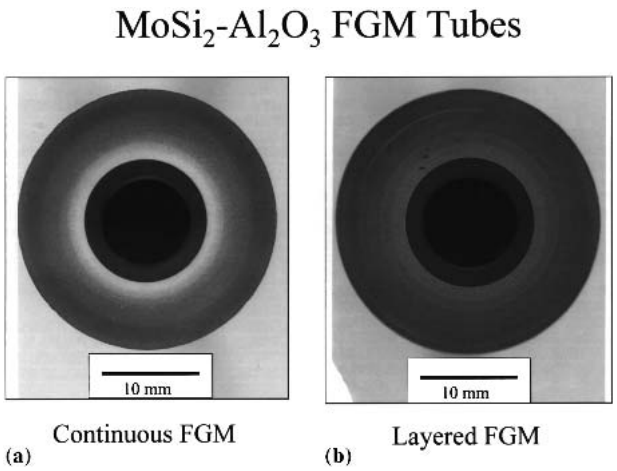

Fig. 3 Optical micrographs of the cross sections of the plasma sprayed FGM tubes. **(a)** Continuous FGM. **(b)** Layered FGM.

$$\sigma_f = \alpha^{-1/\beta}\,\Gamma[1 + 1/\beta] \quad \text{(Eq 6)}$$

$$SD = \alpha^{-1/\beta}\,[\Gamma(1 + 2/\beta) - \Gamma^2(1 + 1/\beta)]^{1/2} \quad \text{(Eq 7)}$$

$$\text{CV} = 100(SD/\sigma_f) \quad \text{(Eq 8)}$$

where $\Gamma(n) = \int e^{-x}\, x^{n-1}\, dx$.

The gamma function was approximated by the equation

$$\Gamma(n) = 3.060 - 4.362n + 3.272n^2 - 1.139n^3 + 0.168n^4 \quad \text{(Eq 9)}$$

The results of the Weibull analysis performed on the composite samples can be seen in Fig. 4. The Weibull modulus (β) for the continuously graded composite samples was significantly higher than the Weibull modulus for the layered/graded samples (13.381 versus 7.635), indicating a smaller scatter in the strength values. The calculated mean Weibull fracture strengths for the composite samples were as follows: continuously graded $MoSi_2/Al_2O_3$ composite, 73.6 MPa; layered and graded $MoSi_2/Al_2O_3$ composite, 69.7 MPa. In comparison, the average

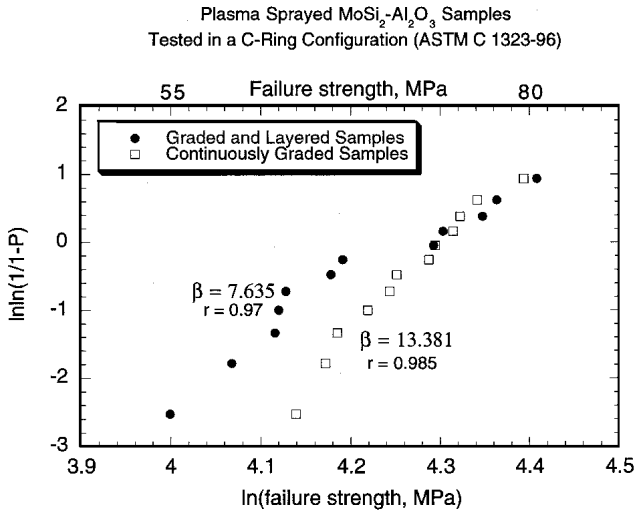

Fig. 4 Weibull probability failure plots obtained from the C-ring tests performed on the FGM samples

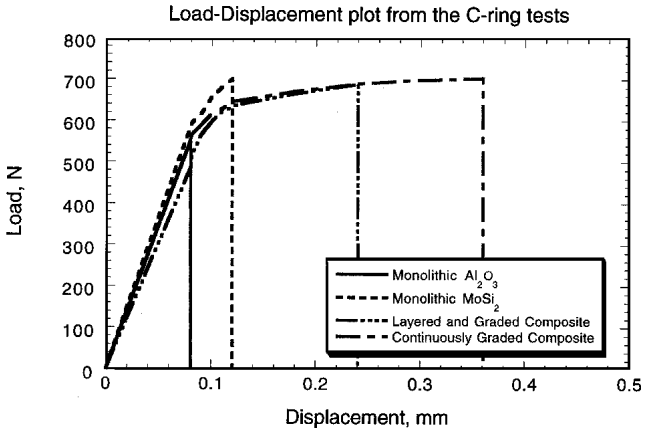

Fig. 5 Load-displacement plots obtained from the C-ring tests performed on the FGM samples

strength values for the monolithic materials were Al_2O_3, 54.5 MPa; $MoSi_2$, 75 MPa. Note that a Weibull analysis was not performed on the monolithic samples because of the limited size (n = 3) of the sample population. The average strength data for the composite samples was very similar to the average strength of the monolithic $MoSi_2$ samples, and significantly higher than that of the monolithic Al_2O_3 samples. The lower strength of the Al_2O_3 samples was attributed to porosity incorporated into the samples during the plasma spraying operation. Image analysis performed on the samples indicated that the monolithic Al_2O_3 samples and the Al_2O_3 within the composite samples had porosity values in the range of 15.3-18.6 v/o. The porosity in the $MoSi_2$ (monolithic and composite) was in the range of 6.8-8.3 v/o. Although the porosity in these samples was higher than one might expect in plasma sprayed structural materials, this porosity is beneficial from a thermal shock perspective. These graded composite samples are being envisaged for thermocouple sheath type applications in glass melting operations, where good thermal shock resistance is an important requirement. It is worthwhile to note that the strength of the composite materials was not

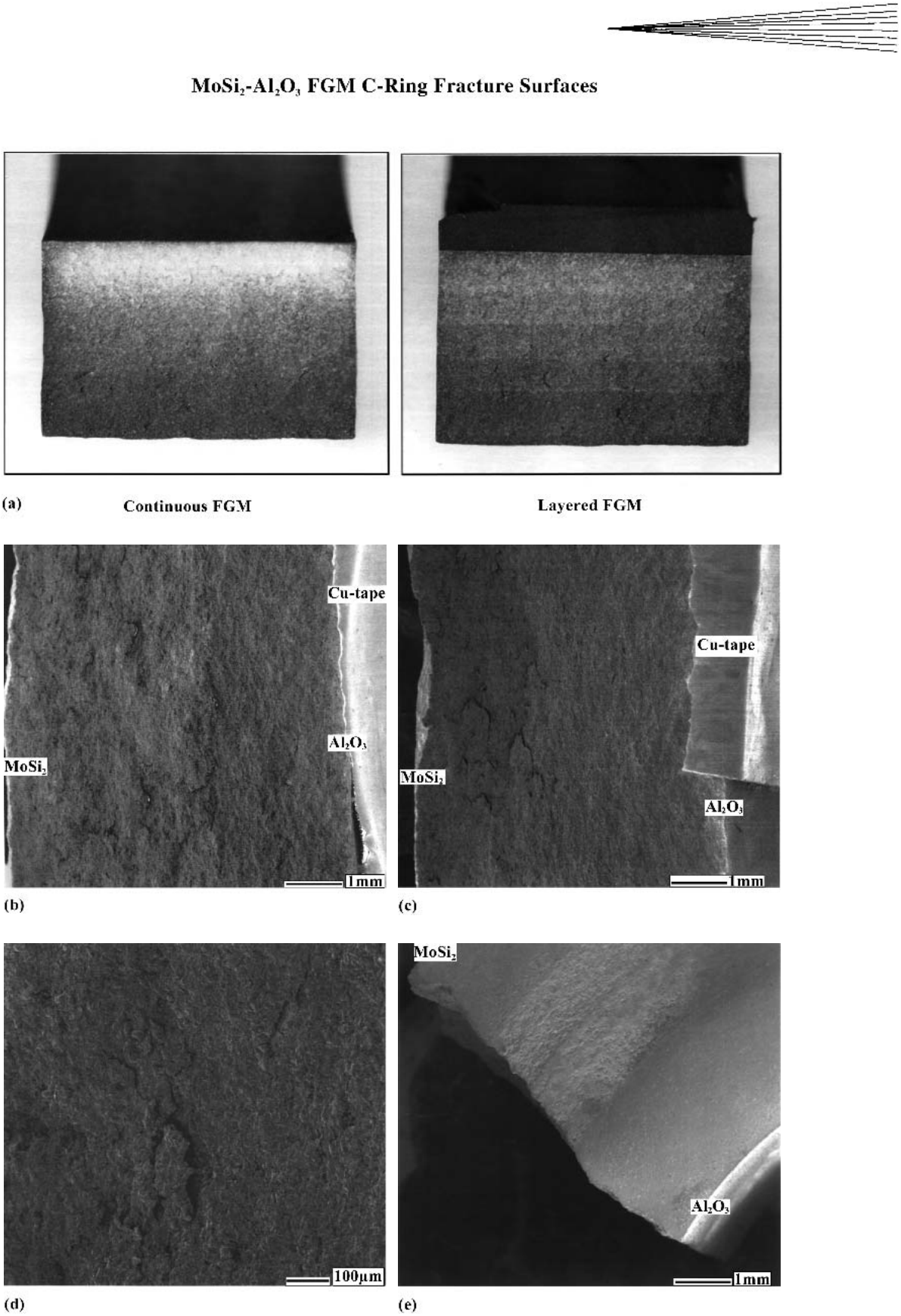

Fig. 6 Fracture surfaces of the C-ring samples. **(a)** Optical micrograph illustrating the overall fracture features. **(b)** Scanning electron micrograph of a continuous FGM fracture surface. Note the change in fracture roughness from the inside to the outside of the sample. **(c)** Scanning electron micrograph of a layered FGM fracture surface. Note the change in fracture roughness from the inside to the outside of the sample. **(d)** High magnification image of the transition region illustrating crack branching. **(e)** Scanning electron micrograph of the side of a continuous FGM fracture sample illustrating the profile of the crack path.

Table 3 Optical Profilometry Results on the Fracture Surfaces of the Samples(a)

	Roughness Parameter R_A Position		
	Al_2O_3-Rich End	Middle	$MoSi_2$-Rich End
Continuously graded	7.35 (0.83)	13.84 (3.2)	6.9 (1.2)
Layered/Graded	7.21 (0.67)	16.2 (2.1)	11.7 (2.4)
Monolithic Al_2O_3	6.87 (0.55)	…	…
Monolithic $MoSi_2$	…	…	5.6 (0.65)

(a) The values are means with the standard deviations in parentheses.

significantly degraded by the presence of the alumina. The strong bonding between the layers is the most likely contributor to strength retention.

Although the strength of the graded composite samples was not significantly improved compared to monolithic $MoSi_2$, the fracture energy of these composite samples was significantly higher than that of monolithic $MoSi_2$. Representative load-displacement curves for the composite samples are compared with those for the monolithic materials in Fig. 5. The average fracture energy values calculated from the area under the load-displacement curves (using the entire specimen fracture area) gave the following values: monolithic Al_2O_3, 285.3 J/m^2; monolithic $MoSi_2$, 496.3 J/m^2; continuously graded $MoSi_2/Al_2O_3$ composite, 955 J/m^2; and layered/graded $MoSi_2/Al_2O_3$ composite, 766.3 J/m^2.

Various assumptions are involved in these calculations: the bonding and load transfer between the layers is assumed to be perfect, the composite is assumed to obey the laws of linear elastic fracture mechanics, and crack propagation in the composite is assumed to be self-similar. Most of these assumptions are true in the case of the composite system.

Enhanced fracture energy of the composite samples was a result of the relatively tortuous path of the crack front during the fracture process. Scanning electron micrographs of the fracture surfaces of the composite samples are shown in Fig. 6(a-e). The crack originates on the tensile surface on the outside of the samples, and propagates toward the inside. The fracture surface starts out smooth and becomes progressively rougher, indicating significant crack deflection. The crack smoothes out as it approaches the inside of the sample (Al_2O_3). The tortuous crack path increases the fracture energy of the composite samples.

Optical profilometry (using a WYKO microscope, Halesowen, United Kingdom) was carried out on the fracture surfaces of the C-rings to quantify differences in the surface roughness of the samples. Three line scans each were performed on a total of eight samples (four continuously graded and four layered/graded). The roughness measurements were done at three points on the line: close to the Al_2O_3 end, in the middle of the sample, and close to the $MoSi_2$ end of the sample. The results of these measurements are given in Table 3. The average surface roughness parameter R_A, which is a measure of the average of the absolute surface deviation from the mean surface contour, was significantly larger in the center of the surfaces of the functionally graded composites. These measurements support the observed increase in fracture energy in these samples compared with the monolithic materials. The increased roughness (and concurrent increase in fracture energy) is a result of extensive crack kinking. Various fracture models have indicated that crack kinking is a strong function of the change in the elastic modulus at the crack tip. Furthermore, the surface roughness in the monolithic regions of the samples (on the inside and outsides of the sample) is significantly smaller compared with the middle of the samples.

4. Conclusions

We demonstrated the capability to produce graded $MoSi_2$-Al_2O_3 composites using conventional plasma spraying equipment. Such composites have a number of applications in the glass industry where the high temperature corrosion and oxidation resistance of $MoSi_2$ coupled with the insulating characteristics of Al_2O_3 have potential use as protective sheaths for thermocouples and other sensors. Although the strength of the graded composite samples was comparable to that of monolithic $MoSi_2$, the fracture energy of the composite was significantly higher than that of the monolithic materials. This improvement in fracture energy (an indirect measure of fracture toughness) is a result of microscopic crack deflection resulting in a tortuous crack path through the material. The low strength of the plasma sprayed Al_2O_3 was attributed to the porosity in the sample. However, the porosity in the Al_2O_3 did not degrade the overall strength of the composite materials.

Acknowledgments

This work was performed at Los Alamos National Laboratory under the auspices of the United States Department of Energy, Office of Industrial Technologies. The authors would like to thank Charles Sorrell for his continuing support. The authors would also like to thank Kendall Hollis and Brian Bartram for their technical assistance with the project.

References

1. A.K. Vasudevan and J.J. Petrovic: "Structural Materials: Properties, Microstructure and Processing," *Mater. Sci. Eng*., 1992, *A155*(1-2), pp. 1-8.
2. J.J. Petrovic: "$MoSi_2$-Based High-Temperature Structural Silicides," *MRS Bull*., 1993, *18*(7), pp. 35-40.
3. J.J. Petrovic and A.K. Vasudevan: "Key Developments in High-Temperature Structural Silicides," *Mater. Sci. Eng*., 1999, *A261*(1-2), pp. 1-5.
4. T.C. Chou and T.G. Nieh: "Mechanisms of $MoSi_2$ Pest During Low-Temperature Oxidation," *J. Mater. Res*., 1993, *8*(1), pp. 214-26.
5. D.A. Berztiss, R.R. Cerchiara, E.A. Gulbransen, F.S. Pettit, and G.H. Meier: "Oxidation of $MoSi_2$ in Comparison With Other Silicide Materials," *Mater. Sci. Eng*., 1992, *A155*(1-2), pp. 165-81.
6. J.J. Petrovic: "Mechanical Behavior of $MoSi_2$ and $MoSi_2$ Composites," *Mater. Sci. Eng*., 1995, *A193*, pp. 31-37.
7. Y.S. Park, D.P. Butt, R.G. Castro, J.J. Petrovic, and W. Johnson: "Durability of Molybdenum Disilicide in Molten Alkali Borosilicate Glass," *Mater. Sci. Eng*., 1999, *A261*(1-2), pp. 278-83.
8. A.H. Bartlett, R.G. Castro, D.P. Butt, H. Kung, and J.J. Petrovic: "Plasma Sprayed $MoSi_2/Al_2O_3$ Laminate Composite Tubes as Lances in Pyrometallurgical Operations," *J. Ind. Heating*, 1996, *63*(1), pp. 33-36.
9. S. Suresh and A. Mortensen: "Functionally Graded Metals and Metal-Ceramic Composites: Thermomechanical Behavior," *Int. Mater. Rev.*, 1997, *42*(3), pp. 85-116.
10. M.P. Rao, A.J. Sanchez-Herencia, G.E. Beltz, R.M. McMeeking, and F.M. Lange: "Laminar Ceramics That Exhibit a Threshold Strength," *Science*, 1999, *286*(5437), pp. 102-05.
11. W.A. Weibull: "A Statistical Distribution Function of Wide Applicability," *J. Appl. Mech*., 1951, *18*(3), pp. 293-97.
12. A.D. Aczel: *Complete Business Statistics*, 2nd ed., Irwin Publishers, Boston, 1993.